

Title: A Defined Heteromeric Kv1 Channel Stabilizes the Intrinsic Pacemaking and Regulates the Efferent Code of Deep Cerebellar Nuclear Neurons to Thalamic Targets

Authors: Saak V. Ovsepian^{1,2}, Volker Steuber³, Marie Le Berre¹, Liam O'Hara¹, Valerie B. O'Leary¹ and J. Oliver Dolly¹

Addresses: (1) International Centre for Neurotherapeutics, Dublin City University, Glasnevin, Dublin 9, Ireland (2) DZNE, Ludwig-Maximilians-Universität München, Zentrum für Neuropathologie, Feodor-Lynen-Str. 23, 81377 München, Germany (3) Science and Technology Research Institute, University of Hertfordshire, College Lane, Hatfield AL10 9AB, UK.

Short title: Kv1 Channel Governs Cerebellar Output to Thalamus

Key words: Kv1 channel; delayed rectifier; antidromic invasion; cerebello-thalamic communication, multi-compartmental modeling

Total number of words: 8168

Corresponding authors: Saak V. Ovsepian or J. Oliver Dolly

Email: saak.ovsepian@dcu.ie or oliver.dolly@dcu.ie

TOC category: Neuroscience – cellular/molecular

ABSTRACT

The output of the cerebellum to the motor axis of the central nervous system is orchestrated mainly by synaptic inputs and intrinsic pacemaker activity of deep cerebellar nuclear (DCN) projection neurons. Herein, we demonstrate that the soma of these cells is enriched with Kv1 channels produced by mandatory multi-merization of Kv1.1, 1.2 α and Kv β 2 subunits. Being constitutively active, the K^+ current (I_{Kv1}) mediated by these channels stabilizes the rate and regulates the temporal precision of self-sustained firing of these neurons. Placed strategically, I_{Kv1} provides a powerful counter-balance to prolonged depolarizing inputs, attenuates the rebound excitation, and dampens the membrane potential bi-stability. Somatic location with low activation threshold render I_{Kv1} instrumental in voltage-dependent de-coupling of the axon initial segment from the cell body of projection neurons, impeding invasion of back-propagating initial segment action potentials into the somato-dendritic compartment. The latter also promotes the dominance of clock like somatic pace-making in driving the regenerative firing activity of these neurons, to encode time variant inputs with high fidelity. Through the use of multi-compartmental modeling and retro-axonal labeling, the physiological significance of the described functions for processing and communication of information from the lateral DCN to thalamic relay nuclei is established.

Abbreviations: PCs - Purkinje cells; DCN - deep cerebellar nuclei; PBS - phosphate buffered saline; PFA - paraformaldehyde; BSA - bovine serum albumin; GS - goat serum; TTX - tetrodotoxin; DTX - dendrotoxin; TsTX-K α - tityustoxin K α ; ISI - inter-spike interval.

INTRODUCTION

Multiple types of voltage-gated K⁺ channels are expressed throughout the nervous system. With distinct activation profiles and kinetics, diversity and differential distribution of K⁺ currents in neurons are vital for regulating numerous functions including resting membrane potential, excitability, spike-frequency adaptation, action potential firing rate and precision (Pongs, 1999; Rudy & McBain, 2001). Of the 8 members of the *Shaker*-related K⁺ channel subfamily (K_v1.1-1.8 α subunits), 7 (with the exception of K_v1.7) have been identified in the nervous system, being particularly enriched on axons, dendrites and soma of different neuron types (Vacher *et al.*, 2008). When expressed in heterologous systems as homo-tetrameric channels, most of these α subunits (K_v1.1, 1.2, 1.5, 1.6 and 1.8) mediate voltage-gated non-inactivating “delayed rectifier” K⁺ currents (*I*K_v1) with others (K_v1.3, 1.4 and 1.7) exhibiting time-dependent inactivation (Stuhmer *et al.*, 1989; Heinemann *et al.*, 1994; Rettig *et al.*, 1994). Distinctively, native K_v1 channels purified from mammalian brain contain homo- or hetero-tetrameric combinations of 4 K_v α forming the aqueous pore, which is associated with 4 ancillary K_v β subunits (Dolly *et al.*, 1994; Scott *et al.*, 1994b), with particular subunit combinations being more favored (Shamotienko *et al.*, 1997; Coleman *et al.*, 1999).

In the cerebellar cortex an unusually high density of K_v1.1, 1.2 and 1.6 α and β 2 subunits observed at the basket cell terminal plexus (McNamara *et al.*, 1993; McCormack *et al.*, 2002; Chung *et al.*, 2005) prompted extensive research into the role of *I*K_v1 in governing the inhibitory synaptic inputs onto Purkinje neurons (PCs) and cerebellum-dependent motor functions (Zhang *et al.*, 1999; McCormack *et al.*, 2002; Herson *et al.*, 2003). Recently, modulation by *I*K_v1 of the dendritic excitability and complex Na⁺/Ca²⁺ burst firing of PCs was documented (Khavandgar *et al.*, 2005; McKay *et al.*, 2005). Surprisingly little, however,

is known about the identity and function of Kv channels in neurons of deep cerebellar nuclei (DCN) since the discovery of a tetraethyl-ammonium-sensitive K⁺ conductance in these cells (Jahnsen, 1986a). Because of the pivotal significance of nuclear projection neurons in relaying balance and coordination-related cerebellar signals to the supra-spinal motor nuclei (Apps & Garwicz, 2005; Ito, 2006), such a lack of information handicaps the advancement of functional models of the cerebellum, given that the physiological properties of individual neurons determine the rules of integration and signal processing by neuronal networks. This deficit of knowledge also complicates the interpretation of evidence, which suggests a significant cerebellar component in neurological phenotypes associated with loss-of-function mutations in genes encoding Kv1.1, 1.2 α and β 2 subunits (Kullmann *et al.*, 2001; Herson *et al.*, 2003; Xie *et al.*, 2011).

The present study defines and functionally characterizes a Kv1 channel composed of Kv1.1, 1.2 α and β 2 subunits in long-range projection neurons of DCN. Evidence is provided for compulsory co-assembly of these subunits into hetero-multimeric channels with their somatic expression to mediate IKv1, which regulates the temporal precision of intrinsic pacemaking, membrane potential bi-stability, rebound firing and axo-somatic integration. These observations substantially advance the current perception of the role of Kv1 channel in the context of cerebellar physiology, with key implications for integrative brain mechanisms.

MATERIALS AND METHODS

Immuno-cytochemistry and microscopy: Experimental procedures conformed to the guidelines approved by the University Ethics Committee and the Irish Authorities. For immuno-cytochemistry, rats (P75-90, n=9) were perfused intra-cardially with phosphate

buffered saline (PBS) (pH 7.4) followed by 4% paraformaldehyde (PFA) in PBS under deep anesthesia (sodium pentobarbital, 200mg/kg, i.p.); brains were fixed overnight in PFA (4°C) and cryo-protected (30% sucrose in PBS, 4°C for 24h). Cerebellum was isolated, frozen and sectioned in the coronal plane (35 µm) (CM3050S, Germany); slices were permeabilized with 0.1% Triton X-100 (in PBS) for 6h (21°C) and blocked for 2h with 10% goat serum (GS), 0.3% bovine serum albumin (BSA) in 0.1% Triton X-100 in PBS. Primary Kv1.X (Kv1.1-1.6 and 1.8) (NeuroMab, USA) or KvβX (Kvβ1-3, 1:10, mouse hybridoma supernatant) monoclonal antibodies were applied for 24h (4°C) in 5% GS, 0.3% BSA, 0.1% Triton X-100 diluted in PBS. After rinsing in 0.1% Tween 20 in PBS (3×20 min), sections were incubated overnight (4°C) with goat anti-mouse Alexa-488 labeled secondary antibody (1:1500). In double-staining experiments, sections exposed to the first (Kv1.2 or β2) primary antibody were washed, blocked and incubated with the second primary Kv1.1 rabbit polyclonal antibody (1:200) (Alomone Lab., Israel) for the same period; after rinsing, they were exposed to goat anti-mouse and anti-rabbit-Alexa fluor 488 or Alexa fluor 594 labeled secondary antibodies (1:1500), washed and mounted. Specificities of the immuno-staining were verified in negative controls, through omission of the primary antibodies. Field micrographs were obtained (20× objective) using laser scanning microscope in epifluorescence mode (pinhole wide open) (AxioObserver, Carl Zeiss, Jena); sub-cellular distributions of Kv1 subunits were analyzed in confocal mode (pinhole = 0.5AU, 40× objective). Argon and Helium/Neon lasers provided the 488nm and 594nm lines for excitation; the emitted signals were sampled in a frame mode at spatial resolution of 30nm/pixel with 1.5µs dwell time. Co-localization of Kv1 subunits (Kv1.1-1.2 and Kv1.1-β2) is defined by the presence of two labels in the same pixel in the digitally-acquired

images, using analytic Zen 2008 software. Well separated emission spectra between Alexa-488nm and Alexa-594nm ensured minimum fluorescence bleed through and accurate assessment of co-localization of Kv1 channel subunits (LSM710 and ConfoCor 3; Zen 2008; Carl Zeiss).

Protein fractionation: For immuno-fractionation, young adult rats (P75-90, n=8) were decapitated under anesthesia (see above); cerebella were removed with the ventro-lateral portion containing lateral nuclei isolated for membrane fraction preparation. Immuno-absorption resins were prepared by covalent coupling of monoclonal antibodies specific for Kv1.X (Kv1.1-1.6) and β 2 subunits to CNBr-activated Sepharose CL-4B (at 2mg of IgG/ml of wet resin) (GE Healthcare Life Science, UK). Extracts of the membrane in non-denaturing lysis buffer containing (mM): Tris HCl, 20; NaCl, 137; EDTA, 2; 10% glycerol; 1% Triton \times 100; pH 8.0 were cleared using a 2h pre-incubation with non-coupled beads before reaction with these antibody-coated resins for 2h (4°C) while rotating. The immuno-absorbed products were eluted using glycine (pH 2.5, 200 mM). Both the flow-through and eluate were subjected to SDS-PAGE and probed with anti-Kv1.X IgGs (1:10). Immuno-reactivity was detected with goat anti-mouse light chain specific secondary antibodies (1:8000) (Jackson Immuno., USA) labeled with horseradish peroxidase (HRP) and enhanced chemiluminescent detection (ECL, Millipore).

Slice preparation and electrophysiological recordings: Recordings were obtained from the lateral nucleus in rat acute cerebellar slices (P9-16; n=46). Animals were deeply anesthetized with ketamine (150mg/kg) and killed by decapitation; the cerebellum was removed and

immersed for 5min in bubbled (95%O₂, 5%CO₂) ice-cold solution containing (in mM): sucrose, 75; NaCl, 85; KCl, 2.5; NaH₂PO₄, 1.25; NaHCO₃, 25; CaCl₂, 0.5; MgCl₂ 4; glucose, 25, pH 7.3. Hemispheres were separated by a central sagittal cut and sliced in the coronal plane (175 μm thick, VT1000S vibratome; Wetzlar, Germany). After 30 min incubation of slices at 32°C in a solution of the same composition, except that sucrose was omitted and the NaCl concentration increased to 125 mM, they were transferred into the recording solution (in mM): NaCl, 125; KCl, 3; NaH₂PO₄, 1.25; NaHCO₃, 25; CaCl₂, 2; MgCl₂, 2; glucose, 25; pH 7.3 and maintained at room temperature (for 6-7h) until used. Recordings were made in a bath fixed to the stage of an upright Zeiss microscope (AxioExaminer NLO-710) under perfusion (~2 ml/min) at temperatures between 31.5-33.0°C. Kynurenic acid and picrotoxin were routinely added to the recording medium (final concentrations 5mM and 0.2mM, respectively) to block fast ionotropic glutamate- and GABA_A/glycineergic-inputs. Patch pipettes (with in-bath input resistance of 4–8 MΩ) were pulled from borosilicate glass (WPI, UK) and for whole-cell experiments filled with intracellular solution containing (in mM): 122 KCH₃O₃S, 9 EGTA, 9 HEPES, 1.8 MgCl₂, 15 sucrose, 14 Tris-creatine PO₄, 4 Mg-ATP, and 0.3 Tris-GTP; pH 7.3 (310 mOsm). Only spontaneously firing neurons of medium and large size (somatic diameter exceeding 10μm) with overshooting spikes and input resistance (R_i , measured by -10pA/500ms pulse from potential close to -65mV) >150 MΩ were included in the analysis. Intrinsic and evoked firing activities were recorded in current-clamp mode, using an EPC10USB amplifier controlled by Patchmaster 2.20 software (HEKA Instruments). Analog signals were filtered at 5 kHz (analog, Bessel filter), digitally sampled at 10 kHz and stored for off-line analysis (PatchMaster, EPC10USB). Bridge balance was implemented and adjusted throughout experiments. Initial (first 5 action potentials),

instantaneous and average (throughout the whole duration of evoked spike trains) discharge rates and inter-spike interval variability (ISI CV) were estimated with event detection macro (Clampfit 10.0, Molecular Devices, CA). The delay of the spike-train was estimated as the time interval between the onset of the depolarizing stimulus and the peak of the first action potential. Amplitudes of the depolarizing plateau potentials were defined as the mean voltage of the last 100ms of the membrane response produced by 1 s depolarizing current-pulse stimulus, after the blockade of Na^+ and Ca^{2+} currents with TTX (0.5 μM) and CoCl_2 (200 μM). The spike train duration was taken as the time window between the peaks of the first and last action potentials evoked by constant current pulse stimulus. The ‘up-state’ time was defined empirically as the period between the first and last crossings of the voltage waveform the threshold potential; the threshold potential was defined as a reference voltage during the upstroke of the first action potential where dV/dt exceeds 5 V/s (Ovsepian & Friel, 2008). Back-propagating spikes were elicited by single or paired-pulse stimulation (intensity 30–50 μA and duration 200 μs) of the axons of projection cells visualized within the peri-nuclear white matter, using two-photon excitation (see below). Under the pharmacological blockade of fast synaptic inputs (to rule out possible effects of K^+ channel blockers through synaptic inputs), the antidromic invasion offers an instructive and reliable electrophysiological model for assessment of the role of somatic voltage-activated $\text{K}_{\text{v}}1$ currents in integration and processing of depolarizing inputs. In cell-attached recording experiments, patch-pipettes were filled with external recording solution, with loose-seal configuration established by positioning the tip of the recording pipette in close proximity to the soma of a DCN neuron and applying slight negative pressure to the electrode (Ovsepian & Friel, 2012). Toxin blockers of $I_{\text{K}_{\text{v}}1}$ were aliquoted in the recording solution, stored at -20°C and added to the

recording medium immediately before use and applied through gravity-driven perfusion lines. DTX_K was purified in-house; TsTX-K α obtained from Peptide International (USA).

Two-photon microscopy and retrograde labeling: Live imaging utilized a NLO710 Axio-Examiner two-photon microscope (Carl Zeiss) based on a mode-locked Ti-sapphire (690-1020 nm) infrared laser (Mai Tai DeepSee, Spectra Physics). Neurons were loaded with bis-fura-2 hexa-K salt (Invitrogen, USA) supplemented to the pipette solution (50 μ M final concentration), which was excited at 760 nm wavelength through a 20 \times water dipping objective (Plan-Apochromat). Emitted photons were collected and sampled by a photomultiplier detector module (NDD, LSM 710), with the output converted into analog voltage at a pixel dwell of 2.31 μ s. All acquisition parameters were controlled by Zen 2008 software (Carl Zeiss). Stacks in Z-dimension were collected from individual neurons over the range of 75-100 μ m with 3D images projected using reconstruction algorithm (Zen 2008). Long-range projection neurons were identified based on their axons extending out of the anatomical borders of the lateral nucleus. For retrograde labeling of projection lateral nuclear neurons, latex micro-spheres (Lumafluor, FL) were pressure injected bi-laterally into the anterior thalamus of 14 day-old rats, using modified stereotactic coordinates (L0.9; P-1.7; D3.6-3.9 mm). In brief, animals (n=7) were anaesthetized with ketamine and xylazine (75 mg/kg and 4 mg/kg, respectively) and the head fixed in the frame. Tracer was infused slowly using a Hamilton micro-syringe equipped with 26S needle (2 μ l in total over 3-4 min). Between 2 and 6 days after injection, the animals were killed under deep anesthesia as described above and used for slice electrophysiology, with labeled neurons visualized using

two-photon excitation (720-740 nm). Tracer injection sites in the anterior thalamus were verified for each experimental animal.

Drugs, data analysis and significance: All drugs and chemicals were obtained from Sigma (Ireland) unless stated otherwise. Data are reported as mean \pm S.E. with statistical significance assessed using paired or unpaired Student's t-test, with $p<0.05$ defining a significant difference.

Multi-compartmental modeling of DCN projection neurons: All computer simulations used a morphologically realistic conductance-based model of an excitatory DCN projection neuron (Luthman *et al.*, 2011; Steuber *et al.*, 2011). The model is based on a morphological reconstruction of a DCN neuron with a large soma (diameter 22 μm) (Steuber *et al.*, 2004) and comprises 517 compartments and eight Hodgkin-Huxley type ion channels: fast and persistent sodium currents, high and low voltage-activated (HVA and LVA) calcium currents, a tonic non-specific cation current providing an inward current to allow spontaneous activity, a purely calcium-gated potassium (SK) current, a hyperpolarization-activated cyclic nucleotide gated (HCN) current, and a mixture of fast and slow delayed rectifier (Kdr) currents. In the absence of sufficient data on the kinetics of Kdr channels in DCN neurons, the fast and slow Kdr current kinetics were based on data from Kv2 and Kv3 channels in globus pallidus neurons (Baranauskas *et al.*, 1999; Baranauskas *et al.*, 2003). The intracellular calcium concentration was modelled as a sub-membrane shell with calcium influx from the HVA current and an exponential decay with a time constant of 70 ms. To replicate the deviation from completely regular spiking that was observed in the absence of

synaptic input in the slice recordings, a diffusive Ornstein-Uhlenbeck (Uhlenbeck & Ornstein, 1930) noise current I_n was added to the soma and modelled as:

$$\frac{dI_n}{dt} = \frac{I_0 - I_n}{\tau_n} + \sqrt{\frac{2\sigma_n^2}{\tau_n}} \eta(t)$$

where $I_0 = 0$ is the mean noise current, $\tau_n = 2\text{ ms}$ is the noise time constant, $\sigma_n = 200$ is the noise standard deviation (SD), and $\eta(t)$ is a random variable drawn from a Gaussian distribution with mean zero and SD one. The simulations were performed using the NEURON simulation software (Hines & Carnevale, 1997). Data analyses were conducted using MATLAB r2008b (The Mathworks). The model that has been used for the simulations will be made available for download from the public ModelDB repository (senselab.med.yale.edu/modeldb/).

Simulations replicated the experimental protocols as closely as possible. The relationship between injected current and initial spike rate was determined after first silencing the spontaneous activity in the model by injecting a hyperpolarizing current (-100 pA), and then measuring the rate over the first five action potentials evoked by varying current injections (20 pA – 300 pA). The antidromic invasion of spikes into the soma was simulated by hyperpolarizing the soma down to varying pre-spike potentials (injected currents between -80 and -180 pA resulted in pre-spike potentials between -63.5 and -75.9 mV), and by measuring the amplitude of the somatic spike or spikelet triggered by stimulating the distal end of the axon hillock 25 μm from the soma with a 5 nA current injection pulse for 200 μs .

RESULTS

Lateral DCN neurons express Kv1.1/1.2 α and β2 subunit-containing K⁺ channels

Rodent DCN encompasses the medial, interpositus and lateral nuclei. Due to the direct relevance of the lateral nucleus to coordination of refined voluntary movements and motor learning (Ito, 1984; Kleim *et al.*, 1998), this study focused on analyses of Kv1 channels therein. Immuno-cytochemistry and confocal microscopy were utilized to assess the presence of Kvα (Kv1.1-1.6 and 1.8) and Kvβ (β1, β2 and β3) subunits, and to visualize their distribution. High levels of immuno-reactivity in the DCN area were detected for Kv1.1, 1.2 and β2 (Fig. 1A, B) with background fluorescence signal for others being indistinguishable from negative controls (not shown). Specificities of Kv1.1, 1.2 α, and β2 labeling were confirmed by omitting the primary antibodies, which abolished the relevant immuno-labeling. Analysis of the sub-cellular distribution of Kv1.1 and 1.2 subunits revealed strong fluorescent co-labeling of the surface membrane, but with also a substantial intracellular presence. Intracellular Kv1.1 was more evident while Kv1.2 labeling was stronger on the surface, where it occurred with Kv1.1 in distinct clusters, especially noticeable in tangential sections (Fig. 1 A2 and Fig. 2A). Notably, the surface expression of both Kv1.1 and 1.2 in all analyzed neurons was restricted primarily to the soma, with rare profiles showing extensions of fluorescence to the proximal processes. Similar observations were made in samples co-labeled for Kv1.1 and β2 subunits, with distinct β2 punctuates also detectable on the cell surface but rarely visible in the cytoplasm (Fig. 1 B2 and Fig. 2B). To ascertain if Kv1.1/1.2 and β2 subunits co-assemble to form channels, their interrelation was analyzed using a co-localization assay and protein immuno-fractionation. Confocal images of double-labeled clusters on the plasmalemma were acquired and the extent of co-expression of the 3 subunits

quantified. As evident (Fig. 2A, B), there is a strong overlap between these proteins (*yellow*) with a high degree of co-localization between Kv1.1 with 1.2 subunits ($92 \pm 6.2\%$; n=78) and Kv1.1 with $\beta 2$ subunits ($76 \pm 5.5\%$; n=89). Tight association of these proteins in channel complexes was confirmed through covalently linking anti-Kv1.1, 1.2 or Kv $\beta 2$ antibodies to Sepharose followed by immuno-fractionation. Indeed, reciprocal absorption with the use of anti-Kv1.1 or 1.2 IgGs indicated hetero-merization of these two α subunits. Hence, each of the anti-Kv1.X-linked antibodies bound their respective subunits: Kv1.1 was eluted from anti-Kv1.1-bound Sepharose and, likewise, Kv1.2 from the anti-Kv1.2-gel (Fig. 2C, D). The absence of both subunits in each respective flow-through confirms that all the Kv1.1 and 1.2 subunits were absorbed by the respective antibody. Probing the products eluted from the anti-Kv1.1 antibody with anti-Kv1.2 IgGs identified Kv1.1-associated Kv1.2 in the eluate, albeit with some Kv1.2 remaining in the flow-through (Fig. 2D). Reciprocally, Kv1.1 was also eluted with Kv1.2 from the anti-Kv1.2 gel, confirming the association of Kv1.1 and 1.2 in heteromeric complexes. However, residual Kv1.1 could be detected also in the flow-through (Fig. 2D). Applying a similar approach but with the use of an anti-Kv $\beta 2$ -coated column, co-assembly of Kv1.1 and 1.2 with $\beta 2$ subunits is demonstrated with, yet again, traces of both Kv1.1 and 1.2 being detected in the flow-through (Fig. 2E). Overall, these data implicate mandatory hetero-tetramerization of Kv1.1 and 1.2 α expressed on the plasma membrane in association with the Kv $\beta 2$ subunit.

***IKV1* regulates the rate and regularity of spontaneous firing of nuclear neurons**

Using cell-attached recordings, the impact of *IKV1* mediated through Kv1.1- and 1.2-containing channels on the intrinsic firing of lateral nuclear neurons was assessed with toxin

blockers (DTX_K 100 nM for $\text{Kv}1.1$ and $\text{TxTX-K}\alpha$ 100nM for $\text{Kv}1.2$) (Wang *et al.*, 1993; Hopkins, 1998). In the presence of kynurenic acid and picrotoxin, most of the cells (92.3%, 24/26) discharged spontaneously in regular mode [range 5-33 Hz, mean $\pm\text{S.E.}$ 17.2 \pm 4Hz; ISI CV range 0.07-0.18, mean $\pm\text{S.E.}$ 0.12 \pm 0.03, n=24]. This activity was accelerated and rendered irregular by DTX_K in 10 of 11 neurons examined (Fig. 3A, D). In the presence of DTX_K both the discharge rate and ISI CV significantly exceeded those of controls (rate increase of 34 \pm 4.2%; CV increase 2.1 fold, n=10; p=0.011). Changes in discharge parameters induced by DTX_K are clearly reflected in the ISI distribution histogram, which became broader and shifted towards a lower ISI (Fig. 3 A2). Comparable firing acceleration and CV increase were found also in neurons exposed to $\text{TxTX-K}\alpha$ (9/9), which enhanced both parameters (31.5 \pm 3.1%, CV 1.9 fold, n=11; p=0.02) (Fig. 3B1-2, D). In 5 neurons after treatment with DTX_K , additional application of $\text{TxTX-K}\alpha$ revealed no further changes in spike rate or ISI variability (rate 32.4 \pm 5.1Hz, CV=0.17 \pm 0.09) (Fig. 3C, D). This observation negates the possible role of $\text{Kv}1.2$ homo-tetramers in spontaneous firing of DCN neurons and suggests mandatory partnership of $\text{Kv}1.2$ with 1.1 in forming functional K^+ channels. Thus, somatically-expressed $\text{Kv}1.1/1.2/\beta 2$ containing channel stabilizes pacemaking and locks the intrinsic spiking of lateral DCN neurons at low and regular rates.

IKv1 dampens the excitability and counter-balances strong depolarizing inputs in lateral DCN neurons

To identify an electrophysiological basis for the acceleration of intrinsic spiking produced by toxins, their effects on depolarization-induced action potential discharge and membrane plateau potentials were analyzed. After the blockade of synaptic inputs, spontaneous spiking

was silenced by a steady negative current, allowing the membrane to respond to depolarizing stimuli from hyperpolarized resting state ($n=16$). In all tested neurons, incrementing depolarizing pulses upon reaching the threshold elicited repetitive firing, which accelerated with increase in the stimulus amplitude and exhibited pronounced adaptation in response to strong stimuli (Fig. 4A). Although similar discharge profiles were also evident in these cells after their exposure to DTX_K, several characteristics of their evoked firing differed from those of the controls. Firstly, DTX_K lowered the threshold current intensity for evoked firing ($24.1 \pm 2.2\text{pA}$ vs. $39.2 \pm 2.5\text{pA}$; 49.6%; $p=0.009$) with the first spike being generated at threshold stimuli and a longer action potential onset delay ($122 \pm 18\text{ms}$ vs. $216 \pm 15\text{ms}$; 77.1%; $n=7$) (Fig. 4B). Secondly, the relation of firing rate to stimulus amplitude was shifted towards lower intensities (Fig. 4C). Finally, treatment of neurons with DTX_K augmented the spike adaptation and reduced the threshold for depolarization-induced block of firing ($178.4 \pm 12\text{pA}$ vs. $124 \pm 9\text{pA}$, 31% decrease; $n=7$; $p=0.012$). These changes produced by DTX_K were accompanied by reduction in the current threshold for rebound discharge (Fig. 4A, lower left inset) and notable upward shift of the inter-spike potentials (sub-threshold membrane depolarizing potential), presumably due to removal of a stabilizing voltage-activated IK_V1 conductance. The latter proposition was tested directly by assessing the effects of toxins on sustained depolarizing membrane potentials after the blockade of Na^+ and Ca^{2+} currents. As illustrated, co-application of TTX ($1\mu\text{M}$) and CoCl₂ ($200\mu\text{M}$) abolished evoked firing, exposing an outward rectification at near-threshold potentials (Fig. 4C). This steady conductance was abated equally by DTX_K or TsTX-K α , as reflected in equivalent increases in the membrane resistance (at $\times 1.8$ threshold current stimulus intensity: DTX_K $33.2 \pm 5\%$, $n=5$; TsTX-K α $28.3 \pm 6\%$, $n=4$) (Fig. 4F). In 4 neurons exposed to DTX_K addition of TsTX-

$\text{K}\alpha$ revealed no further changes in the membrane resistance, consistent with functional occlusion between the two subunits ($\text{DTX}_\text{K} + \text{TsTX-K}\alpha$ $30.1 \pm 7\%$). Overall, the decrease in the current threshold for spike generation along with an increase in the input resistance upon blockade of depolarization-activated IK_v1 appear to underlie the enhancement of evoked firing as well as acceleration of intrinsic pacemaking produced by the toxins.

Rebound firing and membrane potential bi-stability are attenuated by IK_v1

Because sustained depolarization underpins the plateau potentials and membrane potential bistability, the effects of DTX_K on these distinctive traits of DCN neurons were examined (Jahnsen, 1986a; Aizenman & Linden, 1999). After blockade of synaptic inputs and silencing of spontaneous firing by hyperpolarizing currents, anodic break-induced rebound responses were recorded in 9 cells before and after their treatment with DTX_K (threshold I ranging from -60 to -110pA; mean $-73.3 \pm 7.1\text{pA}$) (Fig. 5A). DTX_K (100nM) increased the initial rebound discharge (RD) rate, lowered the RD delay and the threshold current intensity. Figure 5A illustrates RD evoked at $\times 1.4$ threshold stimulus, with DTX_K accelerating its initial rate ($101.5 \pm 9.1\text{Hz}$ vs. $172.3 \pm 10.2\text{Hz}$, $\sim 58\%$; $p=0.006$) and shortening its onset ($48.3 \pm 6.1\text{ms}$ vs. $21.4 \pm 4.2\text{ms}$, $p=0.001$) (Fig. 5B). Quite remarkably, inhibition of IK_v1 also prolonged the duration of the RD with membrane spending longer in the depolarized ‘up-state’ (Fig. 5A). The role of IK_v1 in governing rebound excitation and plateau potentials was also supported by observations from spontaneously firing neurons tested with negative ramp currents before and after exposure to DTX_K ($n=5$). In all these neurons, such stimuli (threshold I ranging from -70 to -180pA; mean $-132.5 \pm 11.2\text{pA}$) transiently blocked the ongoing spiking, an effect followed by robust post-stimulus discharge acceleration (Fig. 5C, D). Notably, DTX_K

in addition to accelerating both pre- and post-stimulus firing, augmented the rebound plateau depolarization and prolonged the time constant for RD rate recovery ($\tau=1.32 \pm 0.3$ s vs. $\tau=4.88 \pm 0.94$ s before and after DTX_K, $p=0.0009$). Similar data were obtained with stimulation of DCN neurons using depolarizing ramps from more negative potentials (mean \pm S.E. -76.4 ± 2 mV, $n=5$). In all experiments, upon reaching the threshold intensity (ranging from +60 to +90pA; mean 78.4 ± 3.1 pA) depolarizing ramps activated a transient discharge, which terminated immediately or shortly after the end of the stimulus (Fig. 5E, left). These brief firing transients contrasted with prolonged plateau responses triggered by comparable stimuli in these neurons after their exposure to DTX_K (Fig. 5E, F). Such augmentation of membrane potential bi-stability along with amplified RD after the blockade of *IKv1* provide strong evidence for its powerful stabilizing influence on voltage dynamics in DCN neurons, with potential impact on processing of both transient and sustained depolarizing inputs.

***IKv1* attenuates axo-somatic integration and promotes clock-like somatic pacemaking**

An important feature of the physiology of DCN projection neurons is the initial segment-somato-dendritic (IS-SD) break on the rising phase of their action potential waveform evoked by antidromic stimulation (Jahnsen, 1986b; Llinas & Muhlethaler, 1988). The absence of such break on spontaneous and current-pulse evoked spike waveforms (Jahnsen, 1986b) suggests that both axonal IS and soma can serve as sites for generation of action potentials in these neurons. Congruently, no IS-SD break was seen in spontaneous action potential waveforms in our current clamp recordings in the presence of fast GABA and glutamatergic synaptic transmission blockers unlike those evoked antodromically displaying a distinct notch at their rising phase (Fig. 6A, 7C-F). Because the antidromic response is typically

recorded at a resting hyperpolarized state and IS-SD transition depends on somatic membrane potential (Coombs *et al.*, 1957), we examined whether the IS-SD break could be unmasked also in spontaneously generated action potentials with gradual hyper-polarization of the soma. In 6 neurons tested, injection of an incremented hyperpolarizing current caused a deceleration of the spontaneous firing rate followed by their complete silencing, with no IS-SD break detected (not shown). Notably, the decline in the firing rate was associated with an increase in ISI variability, with all cells subsequently becoming quiescent displaying pronounced sub-threshold membrane voltage fluctuations, which were abolished by further hyperpolarization (Fig. 6A). Exposure of these cells to DTX_K (100nM) before current injection revealed an increase in firing rate along with strong deterioration of the regularity of spontaneous spiking (Fig. 6B). Injection of incremented hyperpolarizing current caused notable deceleration of their firing with robust increase in ISI CV (Fig. 6B, C). Rather unexpectedly, in 4 neurons numerous distinct sub-threshold ‘spiklets’ of somewhat stable peak amplitude ranging between 12 and 19 mV (n=219 events from 4 individual neurons) also became visible on the background of robust sub-threshold membrane voltage fluctuations (Fig. 6B), with occasional transients of these abortive events into fully blown action potentials (Fig. 6C, D). With few exceptions, the vast majority of cases of transition of ‘spiklets’ into full action potentials revealed a visible IS-SD break at the rising phase of the action potential waveforms. In the presence of pharmacological blockers of fast glutamaergic inputs, these abortive events are likely to represent IS spikes which fail to invade into the soma or occasionally drive full SD action potentials (Fig. 6C). Importantly, analysis of the temporal relation between spontaneously generated abortive spikes and full SD spikes revealed a prominent lag (11.1 ± 0.3 ms; range between 10.2 and 16.4 ms; n=68 pairs of

events) in the time onset of the former after full SD action potentials (Fig. 6D). Because spontaneous abortive spikes occur occasionally at shorter ISI, the lag in their onset after full action potentials is likely to reflect an additional delay introduced by their distal collision with orthodromic action potentials in the axon followed by refractive state of the IS.

Invasion of antidromic action potentials in DCN projection cells are governed by somatic Kv1 channels

To gain further insights into the role of IK_V1 in regulating axo-somatic integration, the effect of DTX_K on invasion of back-propagating spikes from the axon initial segment (IS) to the somato-dendritic (SD) compartment were analyzed. In the presence of blockers of fast synaptic inputs, antidromic responses were evoked by stimulating individual axons visualized within the peri-nuclear white matter of the lateral nucleus, using two-photon microscopy. Shortly after the establishment of a whole-cell configuration with bis-fura 2 supplemented pipettes, cell bodies with dendrites and fine dendritic branches became visible in the majority of neurons (21/26; within 5-7min). Single unperturbed axons extending to the nuclear border also became observable although only in 7 of the neurons (Fig. 7A, B). Incrementing stimulus applied to the axon in all of these cells produced antidromic action potentials in the soma, upon reaching the threshold (30-150 μ A, 200 μ s; mean $78.9 \pm 7.1 \mu$ A); in 6 cells, the latter could be resolved into IS and SD components through varying the somatic membrane potential (Fig. 7C). Maintaining the soma at potentials more negative than -70mV abolished both IS and SD spikes, with neither being detected in controls or after application of DTX_K (Fig. 7C, D top traces). At more positive potentials, however, both IS and SD components were readily evoked, with further depolarization greatly favoring SD

invasion. This relationship between the antidromic response amplitude and somatic membrane potential was notably altered by DTX_K, which promoted SD excitation from more negative potentials without altering the threshold stimulus intensity ($68.3 \pm 5 \mu\text{A}$ vs. $72.4 \pm 6.1 \mu\text{A}$, control and DTX_K, respectively $p=0.29$). Complementary observations were also made through the use of antidromic paired-pulse stimulation, in which DTX_K improved the fidelity of SD spike generation at higher stimuli rates (Fig. 7E, F). As illustrated, DTX_K notably shortened the refractory time for the second SD spike, favoring IS→SD transitions monitored at hyperpolarized potentials (between -55 and -64mV) (Fig. 7F). Improved fidelity and augmented antidromic invasion by *IKv1* blockers indicate the key importance of somatic Kv1 channels in regulating axo-somatic (and perhaps also dendro-somatic) integration and information transfer from DCN to remote targets.

Cerebellar communication with thalamic neurons is governed by somatic *IKv1*

As 70-75% of medium and large neurons of the lateral nucleus project to thalamic structures (Sastry *et al.*, 1997), it was of great relevance to assess directly how *IKv1* influences the output of these neurons. In 7 out of 8 animals bi-laterally injected with a retrograde tracer, punctuate fluorescence was detected in a sizable group of the lateral nuclear neurons (Fig. 8A). Using cell-attached patch recordings, the effects of toxins were analyzed on spontaneous firing of identified projection cells in the presence of synaptic blockers ($n=11$) (Fig. 8B, E, F). Both the discharge rate and ISI variability before treatment (frequency range 6-39 Hz, mean \pm S.E. $20.2 \pm 4\text{Hz}$; ISI CV range 0.09-0.17, mean \pm S.E. 0.14 ± 0.04) were comparable to control values as described above (Fig. 3). In 5 projection neurons exposed to DTX_K, acceleration of spiking with enhancement of ISI CV became noticeable; both the

discharge rate and CV exceeded those recorded prior to treatment (rate increase $32.8 \pm 3.9\%$; CV increase 1.9 fold, $p=0.023$ and $p=0.019$). The remaining 6 cells were tested for the effect of TsTX-K α which proved to be similar to that of DTX $_K$ (rate increase $30.9 \pm 4.8\%$; CV increase 2.1 fold, $n=6$; $p=0.021$; $p=0.016$). Importantly, 4 neurons exposed to TsTX-K α with further application of DTX $_K$ failed to exhibit any visible firing acceleration or ISI variability change, consistent with functional occlusion between Kv1.1 and 1.2 subunits (Fig. 8E, F). Upon examination of 9 thalamus projection neurons with toxins under whole-cell current clamp conditions, in 5 application of DTX $_K$ enhanced the membrane excitability (threshold current: $21.7 \pm 2.1\text{pA}$ vs. $38.2 \pm 3.5\text{pA}$; 44.8% ; $n=5$ $p=0.017$) (Fig. 8 C), shifting the current intensity to discharge frequency relationship towards lower stimulus ranges and higher discharge rates (not shown). Such enhancement of evoked activity was associated with augmented spike adaptation and depolarization-induced blockade of firing, which became prominent at lower current stimulus intensities ($174.4 \pm 14\text{pA}$ vs. $119 \pm 9\text{pA}$, 32% decrease) (Fig. 8 C). In all of these neurons, DTX $_K$ -treatment also enhanced RD and prolonged the sustained rebound spiking ($0.2 \pm 0.14\text{s}$ vs. $8.2 \pm 1.6\text{s}$ $n=5$, $p=0.0008$) (Fig. 8 D). Comparable increases in evoked firing and reduction of the threshold current intensity were obtained from TsTX-K α – treated neurons ($n=4$) with their further co-exposure to DTX $_K$ plus TsTX-K α showing no additional effects (Fig. 8 G). Taken together, the acceleration of spontaneous firing activity with enhanced intrinsic excitability of thalamus projection lateral nuclear neurons caused by DTX $_K$ and TsTX-K α are consistent with an important role of IK_V1 in regulating the efferent code of the cerebellum to thalamic nuclei.

Compartmental model implicates the powerful influence of somatic delayed rectifier IK on excitability, rebound firing and antidromic invasion in DCN projection cells

Kv1.1 and Kv1.2 encode delayed rectifying K⁺ (Kdr) currents with fast and slow activation kinetics, respectively. To further explore the functional role of Kdr currents in DCN neurons, the effect of varying Kdr conductance densities in a morphologically realistic conductance-based model of an excitatory DCN projection neuron (Luthman *et al.*, 2011; Steuber *et al.*, 2011) were examined. To mimic the small deviations from regular spiking that are observed in *in vitro* recordings, a small amount of noise was added to the model (Figure 9, see Methods). A gradual decrease of the conductance densities (GKdr) of both fast and slow Kdr channels in the model resulted in a gradually increased spontaneous spike rate (from 11.3 Hz for 100% of GKdr to 14.0 Hz for 70% of GKdr, Fig. 9A) and inter-spike interval irregularity (CV = 0.11 for 100% of GKdr, CV = 0.36 for 70% of GKdr, Fig. 9B). Decreasing the Kdr conductance density down to 60% of its default value led to non-physiological doublet spiking in the model (spike rate = 16.7 Hz, CV = 0.71, Fig. 9A, B), and a further decrease of GKdr induced depolarization block (not shown). Increasing the conductance density of the Kdr channels led to a small decreases in spike rate and increase in firing regularity (spike rate = 10.7 Hz, CV = 0.09 for 130% of GKdr). Next, the effect of varying Kdr conductance densities on the rebound firing of DCN neurons implicated in information encoding and transmission at the cerebellar output stage (De Schutter & Steuber, 2009; Steuber *et al.*, 2011; Steuber & Jaeger, 2012) was examined. To replicate the experimental findings, rebound responses in the DCN model were simulated after first silencing the spontaneous activity by constant hyperpolarizing current injection (-100 pA), followed by a further injection of -120 pA for 1 s. Figure 9 C, D shows that the Kdr

conductance density regulated both the maximum spike rate and the latency of the rebound response at the offset of the -120 pA current pulse, with rebound spike rates between 40.7 Hz and 141.3 Hz and rebound latencies between 37.1 ms and 38.9 ms for 60 - 130% of the default Kdr conductance density. Moreover, the effect of Kdr channels on the relationship between injected current I and initial spike rate f in the model was examined (see Methods). This simulation was run for the default value of the Kdr conductance density in the model and for 70% of the default value, the lowest value that did not result in non-physiological sustained doublet firing. Figure 9 E shows the resulting $f(I)$ curves, indicating that a partial block of the Kdr conductance can result in an increased gain or slope of the $f(I)$ curve (by 19% from 0.299 Hz/pA to 0.355 Hz/pA). A final simulation investigated how blocking Kdr channels affected the back-propagation of spikes from the axon initial segment into the soma of the model. For both 100% and 70% of the default Kdr conductance density in the model, varying hyperpolarizing currents were injected into the soma to maintain the voltage at a range of negative pre-spike potentials. The distal end of the axon initial segment was stimulated with a brief and strong current pulse (see Methods) and the amplitude of the resulting spikes or spikelets in the soma was measured (Figure 9 F). As shown in Figure 9F, a partial block of the Kdr conductance shifted the lowest somatic prespike potential that could result in full blown somatic action potentials after antidromic invasion of spikes from the axon initial segment to more negative voltages (from -68.2 mV for 100% of GKdr to -69.6 mV for 70% of GKdr), replicating the observations made in experiments with monitoring the effects of DTX_K on antidromic invasion in DCN neurons.

DISCUSSION

Information processing in neurons is regulated by Kv channels whose properties depend on subunit composition. Genetically, the *kcna* (human KCNA) subfamily encodes 8 α subunits (Kv1.1-1.8), inferring an impressive molecular diversity of indigenous Kv1 channels (an estimated 330 combinations assuming binomial tetramerization of these subunit proteins). However, analysis of the content of Kv1 channels from brain extracts has revealed a limited numbers of oligomeric forms, with a prevalence of Kv1.1 and 1.2 α subunits (Scott *et al.*, 1994a; Shamotienko *et al.*, 1997). Such favoritism implies considerable redundancy amongst Kv1 sub-family members and tight regulation of their co-assembly, and accords with greater functionality of Kv1.1 and 1.2 α subunits. Congruously, behavioral studies indicate much more severe neurological phenotypes associated with profound functional impairments in mice affected by deletion of *kcna1* and *kcna2* genes (Smart *et al.*, 1998; Brew *et al.*, 2007) compared to only modestly affected *kcna4* nulls or overtly asymptomatic *kcna3* and *kcna5* knockouts (London *et al.*, 1998; Xu *et al.*, 2000; Archer *et al.*, 2001). Importantly, deletion of *kcna β 2*, a gene which encodes the Kv β 2 ancillary subunit, mimics, although be it milder forms of the neurological phenotype of *kcna1* and *kcna2* nulls (McCormack *et al.*, 2002). Through establishing the molecular identity and functional significance of Kv1 channels in the lateral DCN, the present study demonstrates for the first time enrichment of the soma of projection neurons with Kv1.1, 1.2 α and Kv β 2 subunits and defines the physiological role of the current mediated by these proteins through their mandatory co-assembly. Confined to the soma, IK_V regulates several key activity parameters of these neurons, an observation that could explain the robust phenotypic convergence of neurological symptoms with the high familial penetrance of cerebellar deficit in animals affected by loss-of-function mutations in 3 distinctive K $^{+}$ channel (*kcna1*, *kcna2* and *kcna β 2*) genes.

Molecular identity of Kv1 channels expressed in the lateral cerebellar nucleus

Unlike tetra-domain α subunits of Nav and Cav channels encoded by single genes, the pore of K^+ channels is produced through post-translational tetramerization of 4 individual Kv α subunits. As different combinations of these elementary proteins yield currents with unique biophysical and pharmacological profiles, definition of subunit composition of indigenous K^+ channels in different neuron types is of great physiological and therapeutic relevance. Genetic engineering of recombinant Kv1 tetramers with pre-defined composition followed by their biophysical characterization in heterologous expression systems and correlation with authentic neuronal K^+ currents has recently attracted significant attention (Sack *et al.*, 2008; Al-Sabi *et al.*, 2010). However, the lack of a robust means for translating experimental observations made in heterologous systems to neurons *in situ* imposes major challenges in interpreting the results of these experiments. Another strategy has taken advantage of the differential sensitivity of Kv1 channel subunits to peptide inhibitors, yet again with limitations imposed by relative selectivity of toxin blockers with their inability to differentiate between various stoichiometries of α subunits of Kv channels (Hopkins, 1998; Akhtar *et al.*, 2002). By combining immuno-fluorescence labeling with protein fractionation, the presence and surface expression of co-assembled Kv1.1/1.2 α and Kv β 2 subunits on projection neurons of the lateral DCN is conclusively shown, an observation corroborated by pharmacological data. The absence of other Kv1 α subunits in these neurons is of great physiological interest given that in the mammalian brain Kv1.1 and 1.2 subunits typically tetramerize with other members of the sub-family (Shamotienko *et al.*, 1997; Dodson *et al.*, 2002). Accordingly, the pharmacological data implicate a lack of homomeric Kv1.1 or 1.2

channels in neurons of the lateral nucleus, with DTX_K and TsTXK- α (selective for Kv1.1 and 1.2, respectively) at saturating concentrations affecting equally both the intrinsic pacemaking and excitability of these cells, with no additive effects when co-applied. An endoplasmic reticulum retention motif in Kv1.1, which hinders the surface expression of this subunit alone (Manganas & Trimmer, 2000), could perhaps explain the lack of homomeric Kv1.1 channels in DCN neurons, an interpretation which is also consistent with the deficiency of Kv1.1 homotetramers in brain extracts (Shamotienko *et al.*, 1997). On the other hand, the absence of Kv1.2 homotetramers in the lateral nucleus possessing sparse auto-associative connections (Uusisaari & De Schutter, 2011) accords with well recognized targeting of Kv1.2 subunit-dominated channels to axons and pre-synaptic terminals (Dodson *et al.*, 2003; Vacher *et al.*, 2008). Thus, while multi-merization of Kv1.1/1.2 α subunits yield functional channels of three possible stoichiometries (1:3, 2:2, 3:1), abundance of the Kv β 2 in DCN neurons with its multiple chaperone-like effects on Kv1 α proteins (Shi *et al.*, 1996) could underpin their robust surface expression in the somatic compartment, with powerful physiological effects.

***IKv1* stabilizes pacemaking and regulates the efferent code of nuclear neurons**

From the electrophysiological data presented, it emerges that the *IKv1* regulates pacemaking and reduces the excitability of medium and large size DCN neurons. Acceleration of spontaneous firing and decrease in threshold current intensity for generating action potentials caused by DTX_K or TsTX-K α agree with presented immuno-cytochemical data, which show enrichment of somatic profiles in DCN with Kv1.1 and 1.2 α subunits. To date, *IKv1* has been implicated in firing accommodation and dampening neuronal excitability during strong depolarizing inputs (Locke & Nerbonne, 1997; Dodson *et al.*, 2002; Brew *et al.*, 2007;

Goldberg *et al.*, 2008) as well as in regulating the fidelity of spike propagation in axons and nerve terminal branches (Zhang *et al.*, 1999; Rasband & Shrager, 2000; Dodson *et al.*, 2003). The work presented herein demonstrates, for the first time, somatic expression of Kv1 channels in lateral DCN neurons, which stabilize and lock their intrinsic pacemaking at low and regular rates. As fast excitatory and inhibitory synaptic inputs were eliminated by pharmacological blockers, the acceleration of firing caused by toxins cannot be attributed to dis-inhibition or synaptic excitation of these neurons and suggests a powerful influence of IK_V1 on their intrinsic pacemaking. Unlike earlier work, which analyzed the functionality of DTX-sensitive currents in congenitally silent neurons through their stimulation with prolonged depolarizing current pulses (Locke & Nerbonne, 1997; Dodson *et al.*, 2002; Goldberg *et al.*, 2008), toxin-induced changes in the rate and regularity of intrinsic pacemaking of DCN projection neurons demonstrated herein suggest somatic Kv1 channels being constitutively-active and regulating the output of these cells. In this regard, lateral DCN neurons differ from neighboring cerebellar basket cells and PCs, which also exhibit spontaneous firing albeit being unresponsive to pharmacological blockade of Kv1.1 or Kv1.2 subunit-containing channels or their genetic deletion (Zhang *et al.*, 1999; Herson *et al.*, 2003; Khavandgar *et al.*, 2005; Xie *et al.*, 2011). Differential sub-cellular distribution of IK_V1 in these three neuron types appears to be the most intuitive explanation for such a discrepancy. Indeed, unlike DCN projection neurons enriched with somatic Kv1 channels, in PCs IK_V1 functions appear to be confined to suppression of dendritic hyperexcitability and bursts spiking without notable effects on somatic regenerative tonic firing (Khavandgar *et al.*, 2005; McKay *et al.*, 2005), while in basket neurons these channels are primarily targeted to pre-synaptic terminals (McNamara *et al.*, 1993). Because mechanically-dissociated DCN neurons

in vitro retain spontaneous action potential generation and discharge regularly at rates (Raman *et al.*, 2000) close to those described herein, the self-sustained spiking with its regulation by I_{Kv1} are likely to be inherent somatic functions of these cells. Given that the membrane time constant and input resistance regulate parameters of both spontaneous and evoked firing activity (Hausser & Clark, 1997; Gauck & Jaeger, 2000), toxin-induced alteration of these properties along with a shift of the membrane potential closer to the threshold are likely to underpin the discharge rate acceleration and irregularity in DCN neurons. Such interpretation is consistent with our modeling data in multi-compartmented simulations of DCN neurons, which demonstrated significant increase in the discharge rate and ISI variability associated with downgrading the density of somatic I_{Kdr} . Noteworthy, I_{Kv1} appears to strongly favor the dominance of somatic pacemaking and dampens the antidromic invasion of abortive spikes and voltage fluctuations from the axon initial segment. As demonstrated, blockade of I_{Kv1} promotes invasion of both spontaneous and evoked back propagating spikes and abortive events, which downgrade the precision of intrinsic firing and increase the level of noise in the output of these neurons. A decrease in somatic membrane capacitance due to blockade of near-threshold K^+ conductance could contribute to improved antidromic IS spike invasion (Stuart *et al.*, 1997; Clark *et al.*, 2009) by DTX_K. Conceivably, this or related I_{Kv1} -dependent processes could also govern the dendro-somatic integration and adjust the gain of dendritic inputs to the soma. Moreover, reduced hyperpolarizing drive in the soma would bias membrane potential of the IS towards more depolarizing voltages, greatly increasing the likelihood of generation of occasional IS action potential discharges independently from somatic pacemaker mechanisms. Because DCN cells encode predominantly hyperpolarizing transients produced by GABAergic somatic inputs from PCs,

reduction of near-threshold IK_V1 conductance would strongly downgrade both the timing and threshold for anode break induced excitation in these cells as well as electrical integrity of IS and SD compartments, thereby, disrupting the efferent code of DCN neurons.

Implications for cerebellar functions

The ultimate result of cerebellar integrations is expressed through the projections from DCN neurons to various levels of the neural axis. The fact that these neurons generate output both endogenously and in response to synaptic inputs suggest that they may use their clock-like intrinsic firing for rate-code and coincidence detection in parallel for information processing. Similar to other spontaneously spiking neurons involved in motor coordination, projection cells of DCN accommodate in their efferent code information relayed by inhibitory and excitatory synaptic inputs, through bi-directional alteration of intrinsically generated patterns of activity (Thach, 1968; Eccles, 1973; Gauck & Jaeger, 2000). Through such a mechanism, the wealth of time-variant information from PCs and brain stem inputs is processed by DCN projection cells and conveyed to the nuclei of motor axis with high precision and speed, an important condition for cerebellar control of fine temporal aspects of locomotion and complex voluntary movements (Apps & Garwickz, 2005). Our findings show the powerful influence of IK_V1 on intrinsic pacemaking and its regularity in projection neurons of lateral cerebellar nucleus. In addition, they demonstrate a stabilizing influence of IK_V1 on strong depolarizing inputs with attenuation of anode break induced excitation, membrane potential bi-stability and axo- (and potentially dendro-) somatic integration. Through maintenance the auto-rhythmicity at low and regular rates and dampening the stochastic noise inflicted by near-threshold membrane voltage fluctuations, IK_V1 would reduce the trial-to-trial variability

of the output of projection cells to repeated stimuli, tuning these neurons for encoding functionally relevant synaptic inputs with high temporal precision (Chacron *et al.*, 2003a; Chacron *et al.*, 2003b; Walter *et al.*, 2006). On the other hand, the axo-somatic (and possibly dendro-somatic) de-coupling with attenuation of rebound discharge by IK_V1 is likely to function as a threshold filter, cutting-off sub-threshold signals and sampling only sufficiently strong time variant inputs correlated with physiological processes. Thus, through described herein processes K^+ channels produced by multi-merization of 3 K_V1 subunits (encoded by *kcna1*, *kcna2* and *kcnaβ2* genes) would modulate the end-programs relayed by DCN projection cells to thalamus and other supra-spinal nuclei concerned with balance and coordination of voluntary movements.

FIGURE LEGENDS

Fig. 1: Expression and distribution of Kv1.1/1.2 α and Kv β2 subunits in neurons of the lateral nucleus. (A1) Fluorescence micrographs of the lateral nuclear area labeled individually for Kv1.1 or 1.2 α subunits (top, middle) and merged (bottom). (A2) Sequential confocal optical sections in Z-plane obtained from a representative neuron (top to bottom). Punctuate surface labeling (yellow) corresponds to clustered Kv1.1 and 1.2 subunits (arrows) on the plasmalemma. Note the stronger intracellular Kv1.1 (green) and significant presence of Kv1.2 (red) in surrounding neuropile. (B1) Fluorescence micrographs of the lateral nucleus stained individually for Kv1.1 α or Kv β2 subunits (top and middle) and merged (bottom). Sequential confocal sections in Z-plane obtained from a representative neuron (B2); yellow punctuates on the surface correspond to co-localized Kv1.1 and β2 subunits. Directional arrows: L and D – lateral and dorsal, respectively. MN – medial nucleus

(equivalent to human fastigial nucleus); LN – lateral nucleus (equivalent to human dentate nucleus); IN – interpositus nucleus (equivalent to human emboliform and globose nuclei combined). Calibration scales: 75 μ m (A1 and B1) and 10 μ m (A2 and B2).

Fig. 2: Hetero-multimeric Kv1 channels containing Kv1.1-1.2 α and Kv β 2 subunits are expressed in neurons of the lateral nucleus. (A and B) Confocal micrographs of Kv1 channel-enriched surface clusters illustrate strong overlap between Kv1.1 and 1.2 (A) or Kv1.1 and Kv β 2 (B) subunits. Arrows indicate the interior of the neuron. (C) Immuno-absorption of Kv1.X subunits associated with Kv1.1. After reacting with the detergent extract, DCN tissue with resin containing immobilised anti-Kv1.1 antibody, the resultant eluate (C) proved positive for Kv1.1 and 1.2 (lanes: 3 and 5, respectively) with the flow-through devoid of Kv1.1 (2) but containing residual Kv1.2 (4); Kv1.1 detected in the total extract (6); lane 1 represent protein markers (C). The same procedure was applied using anti-Kv1.2 antibody attached to the resin (D); the eluate showed immuno-reactivity for Kv1.2 and 1.1 (2 and 4, respectively); the flow-through lacked Kv1.2 (1) but possessed a trace of Kv1.1 (3); Kv1.2 in the total extracts (5). (E) Using immobilized anti- β 2 IgGs, the flow-through revealed some Kv1.2 and 1.1 (lanes: 1 and 3, respectively) but the eluate gave stronger staining for Kv1.2 and 1.1 (lanes: 2 and 4, respectively); β 2 in the total extract (5). Arrows indicate the bands of interest.

Fig. 3: IK_{V1} mediated by Kv1.1- or/and 1.2-containing channels stabilizes pacemaking of lateral DCN neurons. (A1, 2) DTX_K accelerates and renders irregular the constitutive firing of nuclear neurons: (A1) representative cell-attached patch recordings [top: before

(left) and in the presence of DTX_K (right)] with graph (bottom) illustrating the time course of the toxin's effect on instantaneous (Inst.) firing rate (FR). Dashed line here and below indicates toxin application period. (A2) Inter-spike interval (ISI) distribution histograms of the same neuron before and after treatment with DTX_K (black and red, respectively). (B1, 2) Representative example of the effect of TsTX-K α on a spontaneous firing neuron: cell-attached recordings before and after toxin treatments (B1, top) with graph of instantaneous firing rate (B1, bottom) and corresponding ISI distribution histograms (B2). (C) Acceleration of spontaneous firing produced by co-application of DTX_K with TsTX-K α : note, further addition of TsTX α (red horizontal bar) after the effect of DTX_K had reached plateau (dashed line), did not cause further increase in the rate of spontaneous firing (bottom). Representative cell-attached recordings before and after toxin treatments are presented as above. (D) A summary plot of the increase in firing rate caused by the blockade of IK_V1 with selective blockers of Kv1.1 or 1.2 α subunits (DTX_K with TsTX-K α applied individually or co-applied (concentrations below histogram bars)). Asterisks here and below highlight statistical significant differences compared to controls.

Fig. 4: IK_V1 attenuates the excitability and counter-balances strong depolarizing membrane potential in DCN neurons. (A) Typical recordings of membrane responses to sub-threshold (bottom), supra-threshold (middle) and strong (>5 times the threshold, top) stimuli before (left) and after (right) DTX_K treatment. Note the lower threshold current (bottom left compared to right), higher discharge rate (middle) and greater spike adaptation with depolarization block produced by strong stimulus (top) in the presence of DTX_K. Horizontal arrows (top) indicate the level of minimal inter-spike potential before application

of DTX_K; insets (bottom left panel) illustrate DTX_K-induced augmentation of rebound discharge in the same neuron (-80pA, 500ms): traces obtained before (black) and after (red) toxin treatment with overlay. (B, C) Relation of stimulus intensity to onset delay of action potential (B) and evoked initial firing rate (C). Note, while DTX_K lowers the current threshold for evoked firing and accelerates the onset of spikes at supra-threshold stimulus intensities, the time to the first spike evoked by threshold stimulus intensity in the presence of DTX_K is longer. Top insets (B and C) illustrate that DTX_K accelerated the spike onset in response to supra-threshold stimulus (B) and enhanced membrane excitability (emergence of slow depolarizing drive) (C, arrow). (D and E) DTX_K augmented sub-threshold membrane depolarization (before I_{NaV} and $ICav$ blockade) and enhanced depolarization induced plateau membrane responses (after I_{NaV} and $ICav$ blockade by TTX and CoCl₂). Horizontal arrows point to the sub-threshold depolarization potential (minimal inter-spike voltage) (D) and sustained (E) potentials before (left) and after (right) application of DTX_K. (F) Summary plot of the estimated membrane resistance (to $\times 2.6$ threshold depolarizing current pulse stimuli). Note that both DTX_K and TsTX-K α applied individually and together notably increase the membrane resistance due to removal of voltage-activated K⁺ conductance.

Fig. 5: Rebound discharge and membrane potential bistability are controlled by IKv1 in DCN neurons. (A, B) DTX_K augments and accelerates anode break induced rebound firing of these neurons. (A) Anode break induced (hyperpolarizing current $\times 2.5$ thresholds) rebound discharge before and after DTX_K (left and middle) and overlay of both (right). Insets below illustrate the initial firing at an expanded time scale. Note acceleration of discharge onset and prolongation of the membrane up-state associated with enhanced rebound firing

caused by DTX_K. (B) Relation of initial (estimated over first 5 action potentials, inset below) rebound discharge rate – rebound discharge delay: measurements represent average estimates of these parameters pooled from individual neurons before and after application of DTX_K. Top inset illustrates the stimulus with a representative evoked response. (C, D) DTX_K accelerated the spontaneous firing and enhanced anode break-induced excitation. Note toxin-induced increase in pre- and post-stimulus firing with prolongation of accelerated rebound firing after the turn-off of the hyperpolarizing ramp stimulus. Raster plots (C, top) from 3 representative neurons collected before and after toxin treatment (left and right, respectively). (D) Summary graph illustrating DTX_K-induced acceleration of intrinsic and rebound firing with delayed post-stimulus firing rate recovery. Inset graph illustrates the rate of the rebound firing frequency recovery in a representative neuron before and after treatment with DTX_K. (E) DTX_K enhances the membrane bi-stability of DCN neurons. Evoked firing induced by brief depolarizing ramp before (left) and after (middle and right) DTX_K treatment. Note robust prolongation of the membrane potential ‘up-state’ caused by sustained post-stimulus depolarization with repetitive firing (right) or plateau potential devoid of action potentials (middle). Left and middle insets illustrate the acceleration of the membrane potential discharge caused by DTX_K (black and red, control and DTX_K, respectively). Inset on the right (arrow) illustrates rapidly-adapting action potentials at expanded time scale with the onset of complete depolarization-induced block of firing. (F) Summary plot of toxin effect on the duration of depolarizing ramp-evoked firing transients (‘up-states’ highlighted by arrows in E, left). Note significant prolongation of the up-state duration after DTX_K treatment within the weaker stimulus ranges.

Fig. 6: Attenuation of axon-derived membrane potential fluctuations by IK_V1 promotes clock-like somatic firing in DCN neurons. (A, B) Continuous current-clamp recordings of membrane potential from a representative DCN neuron: (A, B top) spontaneous firing activity before (A, Control) and after exposure of the same neuron to DTX_K (B, DTX_K). (A, B middle and bottom): recordings of the membrane potential from the same neuron after silencing by injection of incremented hyperpolarizing current. Note emergence of low amplitude membrane potential oscillations (A, middle) at less hyperpolarized potentials which were abolished by further hyperpolarization of the soma (A, bottom). In the presence of DTX_K , the membrane potential fluctuations become more robust (abortive spikes) and occasionally reached to the action potential generation threshold, triggering full somatic spikes. (C) A brief recording episode illustrating somatic and IS generated action potentials in the same neuron with inset below showing the content of the dashed rectangular box at extended time scale. (D) Superimposed recordings of spontaneous activity of DTX_K treated DCN neuron from hyperpolarized potentials revealing occasions of both IS and IS-SD spikes. For illustrative purpose, traces are aligned to reveal the prolonged quiescent phase after the SD spike (also illustrated in the inset raster diagram).

Fig. 7: IK_V1 impedes somatic invasion of antidromic spikes and lowers the fidelity of information transfer at somato-axonal junctions. (A, B) Two-photon micrographs of representative lateral nuclear projection neurons: reconstructed 3D images: (a, b) areas indicated in panel (A) enlarged to illustrate the axon (A, arrows on a) and dendritic segment decorated with rare spine-like elements (A, arrowheads on b). (B) Neuron with clearly visible axon branching local collaterals (arrows) before exiting into the peri-nuclear white matter.

(C) Examples of antidromic spikes with voltage-dependent IS→SD transition before (left) and after (right) the blockade of IK_V1 with DTX_K. Above each trace the membrane potentials at the spike foot are indicated. For illustrative clarity stimulus artifacts are truncated. (D) A summary graph illustrating the relation of antidromic spike amplitude and pre-stimulus somatic potential with representative spikes at decrementing negative somatic potentials (top). (E) Examples of second antidromic spikes evoked by paired-pulse stimulation protocol at incrementing inter-stimulus intervals before (left) and after (right) blockade of IK_V1 with DTX_K. Inter-stimulus intervals are indicated above each trace. (F) A summary graph illustrating the dependence of antidromic spike amplitude on inter-pulse interval and the effect of DTX_K on this parameter. Inset (top) illustrates examples of spikes evoked by paired-pulse stimulation. In the graph, the amplitude of the second spike is expressed as a fraction of the amplitude of the first spike, calculated using the formula $(P_2 - P_1)/P_1$, where P_1 and P_2 are the first and second antidromic action potentials, respectively.

Fig. 8: IK_V1 controls the output of neurons in lateral nucleus to the anterior thalamus.

(A) Schematic of retrograde labeling experiments (left) with a micrograph of live neurons from lateral nucleus (right). Latex beads exhibiting punctuate fluorescence were excited with a two photon laser (730 nm). (B) Cell-attached patch recordings from typical projection neuron [top: before (left) and in DTX_K (right)] with graph (bottom) illustrating the time course of the effect of toxin on instantaneous firing rate and regularity. Dashed line indicates the time window of DTX_K application. (C) Typical recordings of evoked firing from identified projection neuron before and after treatment with DTX_K: stimulus intensities $\times 3.8$ threshold current. Note that DTX_K at this stimulus intensity caused robust augmentation of

spike adaptation (inset, right) with upward shift of the sub-threshold membrane potential and depolarization block. Inset on the left shows the acceleration of the onset of evoked firing by the same treatment. (D) DTX_K prolonged the anodal break-induced rebound discharge in the identified projection neuron: control rebound firing (left) and after DTX_K treatment (right). Inset: summary plot of RD duration before and after treatment of neurons with DTX_K. (E-G) Summary histograms illustrating acceleration of the spontaneous firing rate (E), ISI CV increase (F) and reduction in the intensity of threshold current for evoked firing activity (G) produced by individually applied DTX_K or TsTX α or when co-applied.

Fig. 9: Delayed rectifying K⁺ currents regulate excitability, rebound responses and antidromic action potential invasion in a computational model of a DCN neuron.

In the simulations shown in panels (A – D), the conductance densities of the fast and slow delayed rectifier K⁺ (Kdr) current were varied between 60% and 130% of their default values in the model. (A) Relationship between Kdr conductance and firing rate. (B) Relationship between Kdr conductance and coefficient of variation (CV). (C) Relationship between Kdr conductance and maximum spike rate in the rebound response that followed a -120 pA current injection for 1 s. (D) Relationship between Kdr conductance and latency of the first spike in the rebound response after offset of the -120 pA current injection. (E) Relationship between input current amplitude and initial spike rate (see text and methods) for 100% (solid symbols) and 70% (open symbols) of the Kdr conductance density. (F) Relationship between prespike voltage and somatic spike voltage (see text and methods) for 100% (solid symbols) and 70% (open symbols) of the Kdr conductance density.

REFERENCES

- Aizenman CD & Linden DJ. (1999). Regulation of the rebound depolarization and spontaneous firing patterns of deep nuclear neurons in slices of rat cerebellum. *J Neurophysiol* 82, 1697-1709.
- Akhtar S, Shamotienko O, Papakosta M, Ali F & Dolly JO. (2002). Characteristics of brain Kv1 channels tailored to mimic native counterparts by tandem linkage of alpha subunits: implications for K⁺ channelopathies. *J Biol Chem* 277, 16376-16382.
- Al-Sabi A, Shamotienko O, Dhochartaigh SN, Muniyappa N, Le Berre M, Shaban H, Wang J, Sack JT & Dolly JO. (2010). Arrangement of Kv1 alpha subunits dictates sensitivity to tetraethylammonium. *J Gen Physiol* 136, 273-282.
- Apps R & Garwicz M. (2005). Anatomical and physiological foundations of cerebellar information processing. *Nat Rev Neurosci* 6, 297-311.
- Archer SL, London B, Hampl V, Wu X, Nsair A, Puttagunta L, Hashimoto K, Waite RE & Michelakis ED. (2001). Impairment of hypoxic pulmonary vasoconstriction in mice lacking the voltage-gated potassium channel Kv1.5. *Faseb J* 15, 1801-1803.
- Baranauskas G, Tkatch T, Nagata K, Yeh JZ & Surmeier DJ. (2003). Kv3.4 subunits enhance the repolarizing efficiency of Kv3.1 channels in fast-spiking neurons. *Nat Neurosci* 6, 258-266.
- Baranauskas G, Tkatch T & Surmeier DJ. (1999). Delayed rectifier currents in rat globus pallidus neurons are attributable to Kv2.1 and Kv3.1/3.2 K(+) channels. *J Neurosci* 19, 6394-6404.
- Brew HM, Gittelman JX, Silverstein RS, Hanks TD, Demas VP, Robinson LC, Robbins CA, McKee-Johnson J, Chiu SY, Messing A & Tempel BL. (2007). Seizures and reduced

- life span in mice lacking the potassium channel subunit Kv1.2, but hypoexcitability and enlarged Kv1 currents in auditory neurons. *J Neurophysiol* 98, 1501-1525.
- Chacron MJ, Longtin A & Maler L. (2003a). The effects of spontaneous activity, background noise, and the stimulus ensemble on information transfer in neurons. *Network* 14, 803-824.
- Chacron MJ, Pakdaman K & Longtin A. (2003b). Interspike interval correlations, memory, adaptation, and refractoriness in a leaky integrate-and-fire model with threshold fatigue. *Neural Comput* 15, 253-278.
- Chung YH, Joo KM, Nam RH, Kim YS, Lee WB & Cha CI. (2005). Immunohistochemical study on the distribution of the voltage-gated potassium channels in the gerbil cerebellum. *Neurosci Lett* 374, 58-62.
- Clark BD, Goldberg EM & Rudy B. (2009). Electrogenic tuning of the axon initial segment. *Neuroscientist* 15, 651-668.
- Coleman SK, Newcombe J, Pryke J & Dolly JO. (1999). Subunit composition of Kv1 channels in human CNS. *J Neurochem* 73, 849-858.
- Coombs JS, Curtis DR & Eccles JC. (1957). The interpretation of spike potentials of motoneurones. *J Physiol* 139, 198-231.
- De Schutter E & Steuber V. (2009). Patterns and pauses in Purkinje cell simple spike trains: experiments, modeling and theory. *Neuroscience* 162, 816-826.
- Dodson PD, Barker MC & Forsythe ID. (2002). Two heteromeric Kv1 potassium channels differentially regulate action potential firing. *J Neurosci* 22, 6953-6961.

- Dodson PD, Billups B, Rusznak Z, Szucs G, Barker MC & Forsythe ID. (2003). Presynaptic rat Kv1.2 channels suppress synaptic terminal hyperexcitability following action potential invasion. *J Physiol* 550, 27-33.
- Dolly JO, Rettig J, Scott VE, Parcej DN, Wittkat R, Sewing S & Pongs O. (1994). Oligomeric and subunit structures of neuronal voltage-sensitive K⁺ channels. *Biochem Soc Trans* 22, 473-478.
- Eccles JC. (1973). The cerebellum as a computer: patterns in space and time. *J Physiol* 229, 1-32.
- Gauck V & Jaeger D. (2000). The control of rate and timing of spikes in the deep cerebellar nuclei by inhibition. *J Neurosci* 20, 3006-3016.
- Goldberg EM, Clark BD, Zagha E, Nahmani M, Erisir A & Rudy B. (2008). K⁺ channels at the axon initial segment dampen near-threshold excitability of neocortical fast-spiking GABAergic interneurons. *Neuron* 58, 387-400.
- Hausser M & Clark BA. (1997). Tonic synaptic inhibition modulates neuronal output pattern and spatiotemporal synaptic integration. *Neuron* 19, 665-678.
- Heinemann S, Rettig J, Scott V, Parcej DN, Lorra C, Dolly J & Pongs O. (1994). The inactivation behaviour of voltage-gated K-channels may be determined by association of alpha- and beta-subunits. *J Physiol Paris* 88, 173-180.
- Herson PS, Virk M, Rustay NR, Bond CT, Crabbe JC, Adelman JP & Maylie J. (2003). A mouse model of episodic ataxia type-1. *Nat Neurosci* 6, 378-383.
- Hines ML & Carnevale NT. (1997). The NEURON simulation environment. *Neural Comput* 9, 1179-1209.

- Hopkins WF. (1998). Toxin and subunit specificity of blocking affinity of three peptide toxins for heteromultimeric, voltage-gated potassium channels expressed in Xenopus oocytes. *J Pharmacol Exp Ther* 285, 1051-1060.
- Ito M. (1984). *The Cerebellum and Neural Control*. Raven Press, New York.
- Ito M. (2006). Cerebellar circuitry as a neuronal machine. *Prog Neurobiol* 78, 272-303.
- Jahnsen H. (1986a). Electrophysiological characteristics of neurones in the guinea-pig deep cerebellar nuclei in vitro. *J Physiol* 372, 129-147.
- Jahnsen H. (1986b). Extracellular activation and membrane conductances of neurones in the guinea-pig deep cerebellar nuclei in vitro. *J Physiol* 372, 149-168.
- Khavandgar S, Walter JT, Sageser K & Khodakhah K. (2005). Kv1 channels selectively prevent dendritic hyperexcitability in rat Purkinje cells. *J Physiol* 569, 545-557.
- Kleim JA, Swain RA, Armstrong KA, Napper RM, Jones TA & Greenough WT. (1998). Selective synaptic plasticity within the cerebellar cortex following complex motor skill learning. *Neurobiol Learn Mem* 69, 274-289.
- Kullmann DM, Rea R, Spauschus A & Jouvenceau A. (2001). The inherited episodic ataxias: how well do we understand the disease mechanisms? *Neuroscientist* 7, 80-88.
- Llinas R & Muhlethaler M. (1988). Electrophysiology of guinea-pig cerebellar nuclear cells in the in vitro brain stem-cerebellar preparation. *J Physiol* 404, 241-258.
- Locke RE & Nerbonne JM. (1997). Role of voltage-gated K⁺ currents in mediating the regular-spiking phenotype of callosal-projecting rat visual cortical neurons. *J Neurophysiol* 78, 2321-2335.
- London B, Wang DW, Hill JA & Bennett PB. (1998). The transient outward current in mice lacking the potassium channel gene Kv1.4. *J Physiol* 509 (Pt 1), 171-182.

- Luthman J, Hoebeek FE, Maex R, Davey N, Adams R, De Zeeuw CI & Steuber V. (2011). STD-dependent and independent encoding of input irregularity as spike rate in a computational model of a cerebellar nucleus neuron. *Cerebellum* 10, 667-682.
- Manganas LN & Trimmer JS. (2000). Subunit composition determines Kv1 potassium channel surface expression. *J Biol Chem* 275, 29685-29693.
- McCormack K, Connor JX, Zhou L, Ho LL, Ganetzky B, Chiu SY & Messing A. (2002). Genetic analysis of the mammalian K⁺ channel beta subunit Kvbeta 2 (Kcnab2). *J Biol Chem* 277, 13219-13228.
- McKay BE, Molineux ML, Mehaffey WH & Turner RW. (2005). Kv1 K⁺ channels control Purkinje cell output to facilitate postsynaptic rebound discharge in deep cerebellar neurons. *J Neurosci* 25, 1481-1492.
- McNamara NM, Muniz ZM, Wilkin GP & Dolly JO. (1993). Prominent location of a K⁺ channel containing the alpha subunit Kv 1.2 in the basket cell nerve terminals of rat cerebellum. *Neuroscience* 57, 1039-1045.
- Ovsepian SV & Friel DD. (2008). The leaner P/Q-type calcium channel mutation renders cerebellar Purkinje neurons hyper-excitable and eliminates Ca²⁺-Na⁺ spike bursts. *Eur J Neurosci* 27, 93-103.
- Ovsepian SV & Friel DD. (2012). Enhanced synaptic inhibition disrupts the efferent code of cerebellar Purkinje neurons in leaner Cav2.1 Ca 2+ channel mutant mice. *Cerebellum* 11, 666-680.
- Pongs O. (1999). Voltage-gated potassium channels: from hyperexcitability to excitement. *FEBS Lett* 452, 31-35.

- Raman IM, Gustafson AE & Padgett D. (2000). Ionic currents and spontaneous firing in neurons isolated from the cerebellar nuclei. *J Neurosci* 20, 9004-9016.
- Rasband MN & Shrager P. (2000). Ion channel sequestration in central nervous system axons. *J Physiol* 525 Pt 1, 63-73.
- Rettig J, Heinemann SH, Wunder F, Lorra C, Parcej DN, Dolly JO & Pongs O. (1994). Inactivation properties of voltage-gated K⁺ channels altered by presence of beta-subunit. *Nature* 369, 289-294.
- Rudy B & McBain CJ. (2001). Kv3 channels: voltage-gated K⁺ channels designed for high-frequency repetitive firing. *Trends Neurosci* 24, 517-526.
- Sack JT, Shamotienko O & Dolly JO. (2008). How to validate a heteromeric ion channel drug target: assessing proper expression of concatenated subunits. *J Gen Physiol* 131, 415-420.
- Sastray BR, Morishita W, Yip S & Shew T. (1997). GABAergic transmission in deep cerebellar nuclei. *Prog Neurobiol* 53, 259-271.
- Scott VE, Muniz ZM, Sewing S, Lichtenhagen R, Parcej DN, Pongs O & Dolly JO. (1994a). Antibodies specific for distinct Kv subunits unveil a heterooligomeric basis for subtypes of alpha-dendrotoxin-sensitive K⁺ channels in bovine brain. *Biochemistry* 33, 1617-1623.
- Scott VE, Rettig J, Parcej DN, Keen JN, Findlay JB, Pongs O & Dolly JO. (1994b). Primary structure of a beta subunit of alpha-dendrotoxin-sensitive K⁺ channels from bovine brain. *Proc Natl Acad Sci U S A* 91, 1637-1641.

- Shamotienko OG, Parcej DN & Dolly JO. (1997). Subunit combinations defined for K⁺ channel Kv1 subtypes in synaptic membranes from bovine brain. *Biochemistry* 36, 8195-8201.
- Shi G, Nakahira K, Hammond S, Rhodes KJ, Schechter LE & Trimmer JS. (1996). Beta subunits promote K⁺ channel surface expression through effects early in biosynthesis. *Neuron* 16, 843-852.
- Smart SL, Lopantsev V, Zhang CL, Robbins CA, Wang H, Chiu SY, Schwartzkroin PA, Messing A & Tempel BL. (1998). Deletion of the K(V)1.1 potassium channel causes epilepsy in mice. *Neuron* 20, 809-819.
- Steuber V, De Schutter E & Jaeger D. (2004). Passive models of neurons in the deep cerebellar nuclei: the effect of reconstruction errors. *Neurocomputing* 58, 563-568.
- Steuber V & Jaeger D. (2012). Modeling the generation of output by the cerebellar nuclei. *Neural Networks* In press.
- Steuber V, Schultheiss NW, Silver RA, De Schutter E & Jaeger D. (2011). Determinants of synaptic integration and heterogeneity in rebound firing explored with data-driven models of deep cerebellar nucleus cells. *J Comput Neurosci* 30, 633-658.
- Stuart G, Spruston N, Sakmann B & Häusser M. (1997). Action potential initiation and backpropagation in neurons of the mammalian CNS. *Trends Neurosci* 20, 125-131.
- Stuhmer W, Ruppertsberg JP, Schroter KH, Sakmann B, Stocker M, Giese KP, Perschke A, Baumann A & Pongs O. (1989). Molecular basis of functional diversity of voltage-gated potassium channels in mammalian brain. *Embo J* 8, 3235-3244.
- Thach WT. (1968). Discharge of Purkinje and cerebellar nuclear neurons during rapidly alternating arm movements in the monkey. *J Neurophysiol* 31, 785-797.

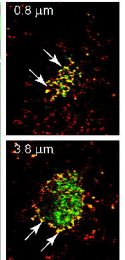
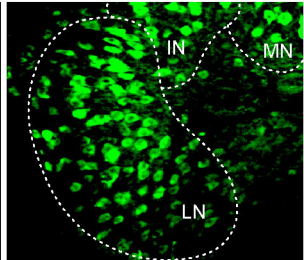
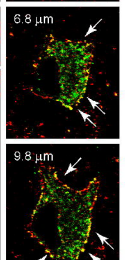
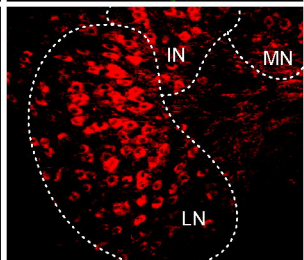
- Uhlenbeck GE & Ornstein LS. (1930). On the theory of the Brownian motion. *Physical Review* 36, 823-841.
- Uusisaari M & De Schutter E. (2011). The mysterious microcircuitry of the cerebellar nuclei. *J Physiol* 589, 3441-3457.
- Vacher H, Mohapatra DP & Trimmer JS. (2008). Localization and targeting of voltage-dependent ion channels in mammalian central neurons. *Physiol Rev* 88, 1407-1447.
- Walter JT, Alvina K, Womack MD, Chevez C & Khodakhah K. (2006). Decreases in the precision of Purkinje cell pacemaking cause cerebellar dysfunction and ataxia. *Nat Neurosci* 9, 389-397.
- Wang H, Kunkel DD, Martin TM, Schwartzkroin PA & Tempel BL. (1993). Heteromultimeric K⁺ channels in terminal and juxtaparanodal regions of neurons. *Nature* 365, 75-79.
- Xie G, Harrison J, Clapcote SJ, Huang Y, Zhang JY, Wang LY & Roder JC. (2011). A new Kv1.2 channelopathy underlying cerebellar ataxia. *J Biol Chem* 285, 32160-32173.
- Xu C, Tang G, Lu Y & Wang R. (2000). Molecular basis of voltage-dependent delayed rectifier K⁺ channels in smooth muscle cells from rat tail artery. *Life Sci* 66, 2023-2033.
- Zhang CL, Messing A & Chiu SY. (1999). Specific alteration of spontaneous GABAergic inhibition in cerebellar purkinje cells in mice lacking the potassium channel Kv1. 1. *J Neurosci* 19, 2852-2864.

A1

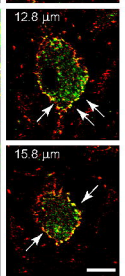
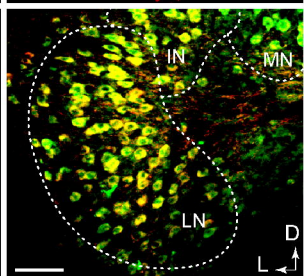
A2

B1

B2

Kv1.1 α subunitKv1.2 α subunit

Merged



Merged

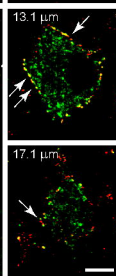
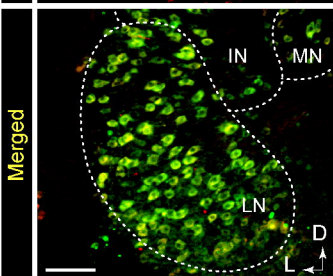
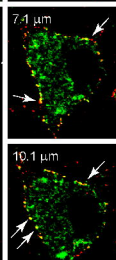
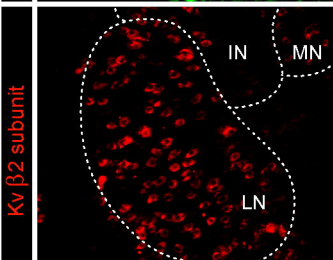
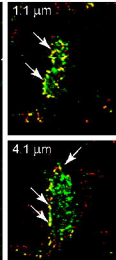
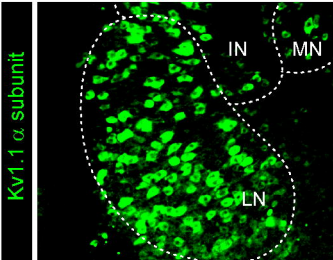


Figure 1, Ovsepian et al.,

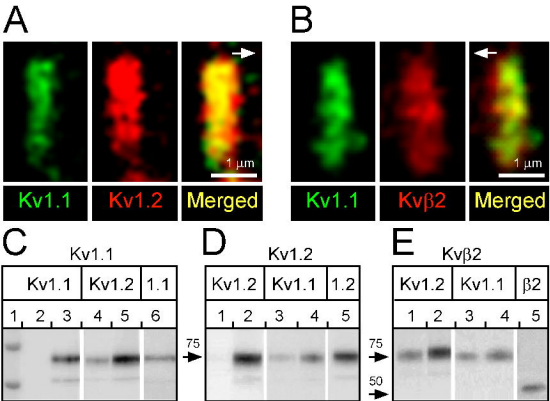


Figure 2, Ovsepian et al.,

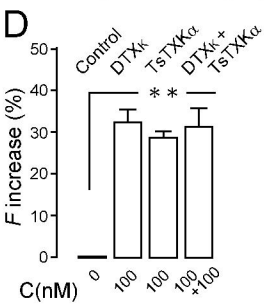
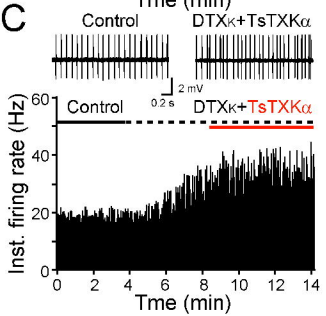
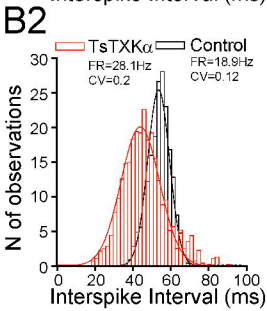
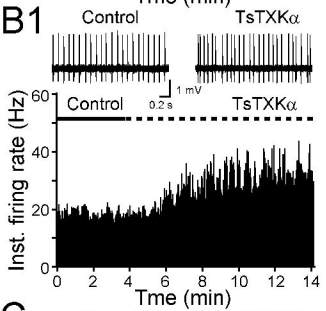
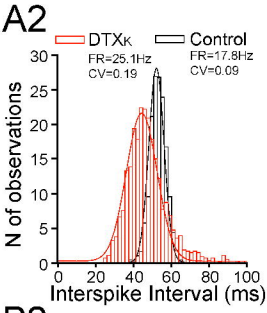
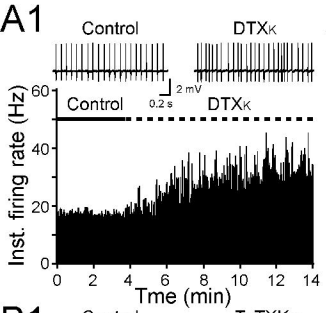


Figure 3, Ovsepian et al.,

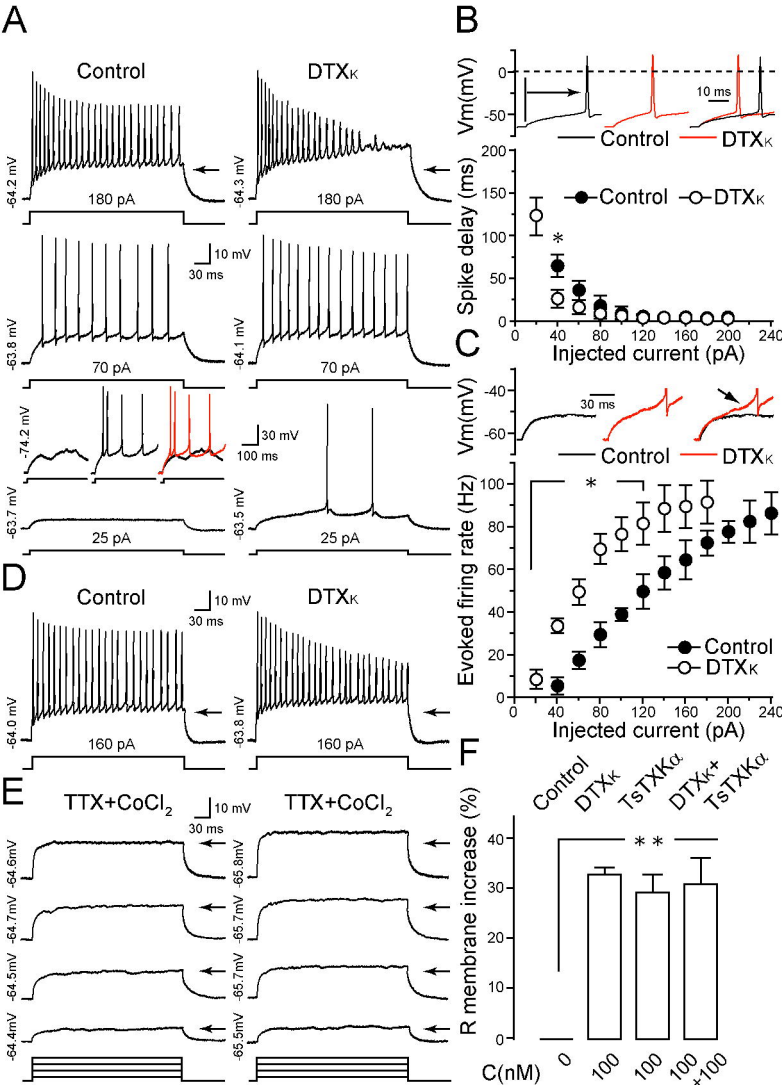


Figure 4, Ovsepian et al.,

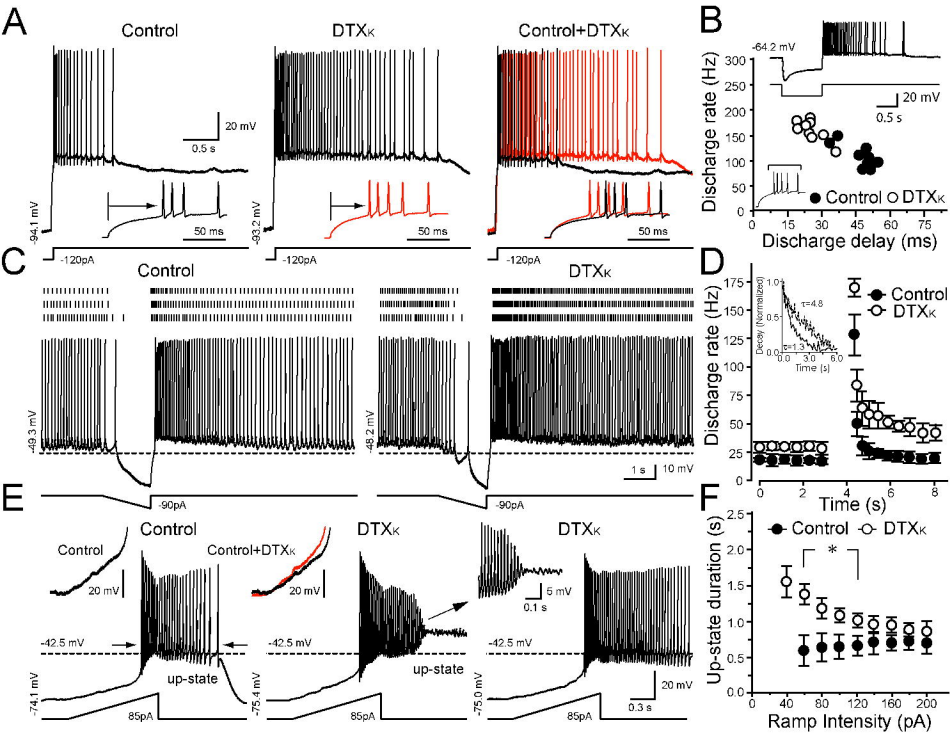


Figure 5, Ovsepian et al.,

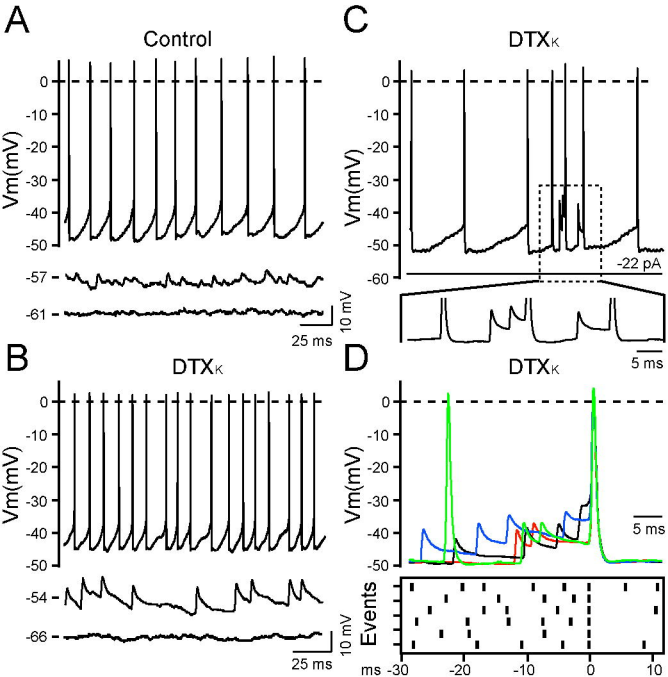


Figure 6, Ovsepian et al.,

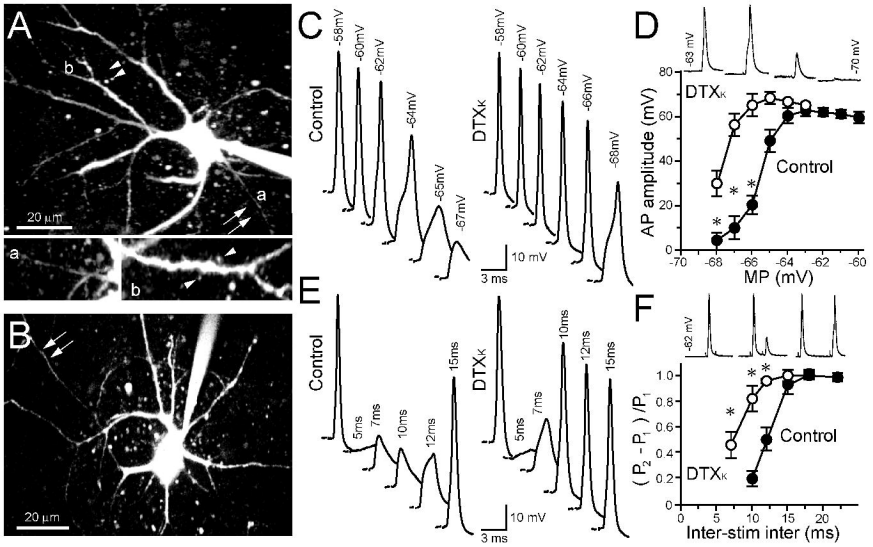


Figure 7, Ovsepian et al.,

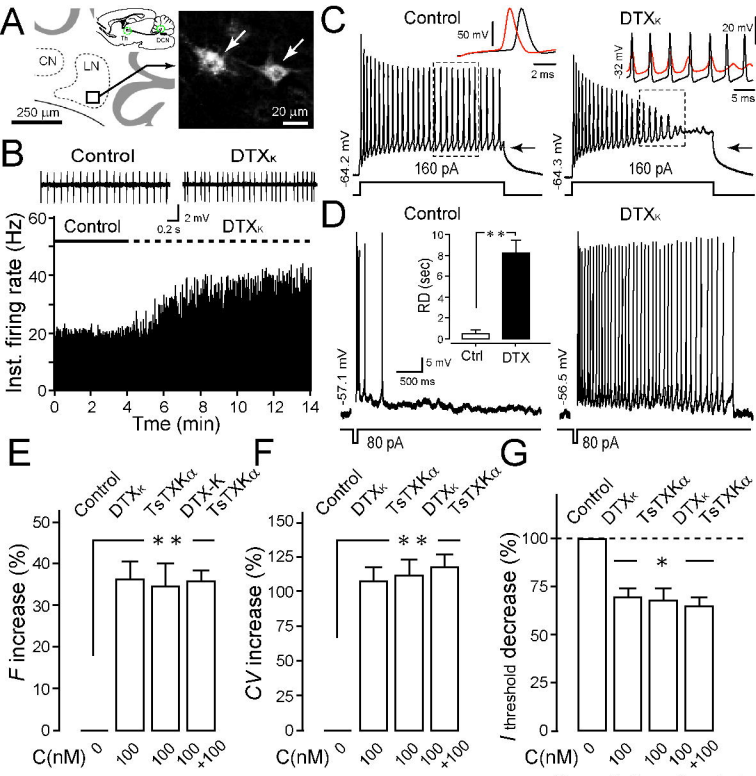


Figure 8, Ovsepian et al.,

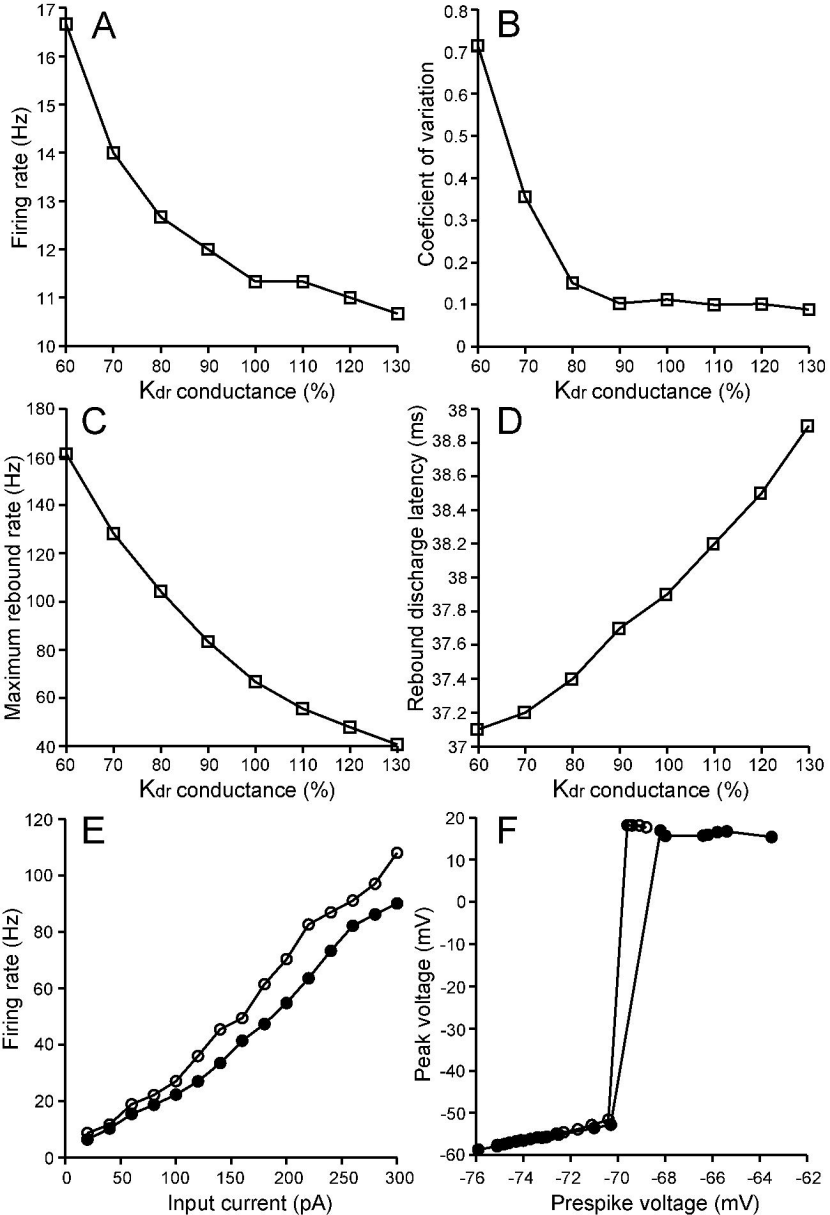


Figure 9, Ovsepian et al.,